Finite-difference modelling of near-surface effects

Peter M. Manning and Gary F. Margrave

A colour version of this paper is available on the CREWES 2001 Research Report CD.

ABSTRACT

A two-dimensional finite-difference modelling program with an accurate free surface representation was used to model dynamite-style records. The results depict the recording of near-surface effects and their relationships to the recording of body waves. For body waves, the source ghost is shown to cause an approximate derivative wavelet, where the precise phase rotation depends on the depth of the source. The character of the first breaks is shown to depend on the near-surface velocity profile, affecting their amplitude, arrival time, and dispersion. The dependence increases as the offset increases. A preliminary study of the effect of an unbalanced compression source is given.

INTRODUCTION

The study was begun after a series of correspondences with Peter Cary on the use of first breaks to determine polarity of seismic data. The object was to simulate the change of first breaks with offset, and to see if model results would be consistent with the first-break polarity determinations commonly assumed. The polarity convention is to plot the first breaks as troughs in order to display positive reflections as peaks. The work was done with the code developed to model surface waves (Manning & Margrave 1998). A staggered grid was used without any correction factors for dispersion or stability.

MODEL PARAMETERS

All models were initiated from a compression source with left/right symmetry at the left edge of the display and so only the right half of the symmetric results were shown. The top of the model was a flat, ideal free surface. The bottom of the model was perfectly rigid, and the reflections from it were used as the representation of a positive reflection coefficient. The right edge of the model was affected by code that attempted to eliminate reflections, and succeeded quite well where the velocities next to the edge were the basic half-space velocities (described below).

The models used numbers that are realistic as metric units in the earth. The sample rates in the x and z directions were then 2 metres, and the sample rate in time was 0.4 milliseconds. The basic half-space velocities were 1600m/s for pressure waves and 800m/s for shear waves. These were modified for later models to provide velocity steps and gradients. The sample rates were fine enough to model the pressure waves accurately, but the surface waves can be seen to have some numerical dispersion.

The energy source was a 30Hz zero-phase Ricker wavelet applied from zero time at the 0.4ms sample rate. A displacement specified by the wavelet was applied at the same time to right and left (+x- and –x-directions) at adjacent sample points. It was

also applied down and up (+z- and –z-directions) at the staggered grid z positions which were symmetric to the x positions. The displacements applied at a given time were all identical except for the simulated unbalanced source, where the up displacement (-z direction) was reduced to 0.9 of the other three displacements.

The resulting surface recordings are all from vertical geophones. Snapshots at a time halfway through each surface recording give an idea of what is happening within the earth. The events within the earth are coded with three main symbols: R for Rayleigh waves, P for pressure waves, and S for shear waves. The detailed codes are as follows: Pd for the direct pressure wave, Pr for the reflected pressure wave (with ghost energy), Sg for the shear wave ghost off the surface, Scs for the shear energy converted from the direct pressure wave at the surface, and Scr for the shear wave converted upon reflection.

The 2001 CREWES Research Report CD includes movies of wave propagation for some of the more definitive models.

CONVENTIONAL MODEL RESULTS

Case 1

The base model case had the energy source at 8 metres within a uniform half-space and the surface recording is shown in Figure 1. The zero-phase Ricker wavelet used appears as a first break at zero-offset (marked with an R). The reflection at 280 ms. can be seen as a combination of the primary wave at 275ms. (marked P), and the ghost at 285ms. (marked G). The brackets show that the effective length of the composite wavelet has not changed much from near offsets to an offset of 350m. The ground roll dispersion is caused mainly by inadequate sampling.

A snapshot of this model at a time of 200 milliseconds is shown in Figure 2. The weak first breaks are at about 270 metres. The compressional reflection Pr is propagating upwards.

Case 2

The second case was identical to the first except that the energy source was placed at 18 metres, and the surface recording is shown in Figure 3. At the left, the Ricker wavelet is again marked with an R, the primary reflection with a P, and the ghost reflection with a G. The primary then appears at shorter time, and the ghost at longer time. The advantage of this deeper shot is reduced ground roll. The disadvantage is that the greater separation of the primary and ghost reflections causes the composite reflection to have a lower frequency and the frequency content to change with offset. This can be seen from the shorter wavelength at the longer offsets for the composite primary/ghost wavelet (shown by the brackets). The change of frequency with offset shown here occurs along shallow reflectors, and the effect is reduced as the depth of the reflectors increase. A trace at long offsets will have an inconsistent set of frequency lowered reflections, ranging from minimum lowering at shallow times to the equivalent of zero offset lowering at deeper times. The inconsistency severely limits the effectiveness of a statistical deconvolution on these individual traces. A

study of this effect with the real Blackfoot data can be seen in Hamarbitan & Margrave (2001).

Inspection of Figures 1 and 3 shows results that are consistent with the standard polarity convention. The first break energy is plotted as a zero-phase trough, and the reflection from the positive impedance change is a close approximation to a zero-phase peak. The interacting mechanisms to explain this are quite complex, but part of the explanation is that the reflection wavelet combines a primary and a ghost.

Case 3

This model has a source at 8 metres as in case 1, but has a velocity gradient of 1600 to 1920m/sec over a depth range of 20 to 60 metres. This causes the raypaths and wavefronts to curve upward and provides much more energy to the first breaks. A snapshot of the model after 200 milliseconds is shown in Figure 6. The higher energy of the wavefront is shown by the higher colour intensity, and the greater component of energy in the vertical direction results in higher amplitude recording at the vertical geophones.

The surface recording from this model is shown in Figure 5. The higher first-break amplitudes at longer offsets are obvious. Close inspection shows a curve toward shorter times with longer offsets, also caused by the velocity gradient. Inspection also shows the first breaks starting to spread out, caused by energy arrival through more than one unique path.

Case 4

This model has the velocity gradient of case 3 and the 18-metre-deep shot of case 2. A surface recording is shown in Figure 7 and a snapshot in Figure 8. All the first break characteristics of case 3 can be seen here as well. The first breaks at longer offsets tend to be higher amplitude, more dispersed, and arrive at shorter times because of the velocity gradient.

Case 5

This model is similar to case 3 except that the velocity gradient was replaced by a velocity step, from 1600 to 1920m/sec. at 40 metres. The shot depth was at 8 metres. The surface recording from this model is shown in Figure 9, and a snapshot in Figure 10.

The features of this model are similar to those of the velocity gradient case of Figure 5 but with several differences. The first break times are not curved, but show an abrupt change in slope at 125 metres. At about the same offset the amplitudes increase, and then show a gradual reduction. It is evident that the first break dispersion is caused by interference between the energy that travelled through the high-speed layer and the remnants of energy that arrived directly through the slower shallow layer.

Multiple reflections also appear, caused by the velocity step. A multiply reflected first break is just beginning to show at the longest offsets. Also a primary refection is visible at short offsets, and multiples behind the main reflector.

Case 6

This model duplicates the conditions in the earth of case 5 but with the energy source at 18 metres. The surface recording from this model is shown in Figure 11, and the snapshot in Figure 12.

The subtle effects that show in the shallow source of case 5 are also evident in this case. The higher first break amplitudes tend to make the first break multiples more obvious. These are caused by wave packages that reflect between the surface and the higher speed layer at 40 metres. The snapshot also shows a conversion event from this interface.

UNBALANCED PRESSURE SOURCE

An unbalanced pressure source was examined for the type of waves that it propagated, and then used as the source within the model of case 2 (with an 18-metre source depth as with the Blackfoot data). The means of generating the unbalanced source is described in the model parameters section.

A real world pressure-wave source cannot be expected to apply exactly the same pressure on the surrounding rock in all directions with every shot. In particular, it seems likely that the coupling directly above the shot, where the shot hole is open, would not be as effective as at the sides or down toward the bottom of the hole. For this reason, an unbalanced shot was assumed to apply less force in the upward direction.

A pressure wave that displaces adjacent sections of the earth with different amplitudes will cause shear stresses between these sections. The stressed sections must then radiate shear waves. The question then is whether the shear waves will cancel each other out, or reinforce each other and propagate in a stable or partly stable way. The numerical simulation tried here suggests that these shear waves are stable for a time long enough to affect normal seismic records.

The main deficiency with the models shown here is that a three-dimensional world is simulated with a two-dimensional model (a model assuming no changes in the y direction). These models will be particularly inadequate near the source, where the variation in the y direction will be most important. Still, they may be of some qualitative use.

SHEAR WAVE FROM THE UNBALANCED SOURCE

An example of a shear wave generated from an unbalanced source in the middle of a uniform material is shown in Figure 13. It occurs because the upward displacement amplitudes are 0.9 of the amplitudes in the horizontal and downward directions. The

originating pressure wave appears as the lighter coloured circles that have almost reached the boundaries (marked P). Its energy has spread over the upper portion (it has healed enough) so that it cannot be distinguished from a balanced wave.

The unbalanced shear wave component (marked with an S) has higher amplitudes than the pressure wave because it has not spread as much. Its displacements in the z direction are symmetric about a z-axis through the centre of the plot, and its displacements in the x direction are anti-symmetric about this same axis. The two sides face each other across smoothed discontinuities at the top and bottom. Note that the high opposing amplitudes approach each other quite closely.

For comparison, a pure cylindrical shear wave from the same frequency source wavelet is shown in Figure 14. This type of wave has no zeros along the propagating ring and displacement amplitudes are uniform all the way around.

BLACKFOOT DATA UNBALANCED

Figure 15 shows a high-quality radial record from the Blackfoot area that has been scaled to show the near surface events. The corresponding vertical record is shown in Figure 16. The events marked by the blue lines are proposed to be direct arrivals of unbalanced shear energy. The reasons are as follows:

- The motion is in a pure shear direction (little on the vertical record).
- The slopes are reasonable for shear velocities (700m/sec).
- The events tend to be anti-symmetric about the source.
- The anti-symmetric events still have high amplitude near the source.

An attempt was made to model the surface recording of unbalanced shear energy and the results are shown in Figure 17. They show the shear energy converting into ground roll at the surface with very high efficiency, an effect not seen on the real records. The difference can be explained by the limitations of two-dimensional modelling in simulating three-dimensional data. In the real 3-D case, the shear energy probably has too much curvature in the surface plane to convert to ground roll near the source. Rayleigh developed the original surface-wave theory for 2-D cases, and significant curvature perpendicular to the wave profile invalidates the assumptions. Minimal curvature is probably required to propagate at all. As the distance from the source increases the curvature at the surface will decrease, and the high conversion rate from shear to ground roll predicted by the usual cylindrical model will become more realistic.

CONCLUSIONS

Finite-difference modelling with an accurate free-surface representation can give insight into the relationship of the conventional reflections caused by body waves, and the waves affected by boundaries, like first breaks and ground roll. In particular:

- The model results are consistent with the polarity conventions established for standard geophysical processing.

- Reflection changes can be related to depth of shot through ghosting effects, and can explain how reflections become lower frequency and resist deconvolution application.

- Near-surface velocity structure can be related to the first break character changes of amplitude, arrival time, and dispersion.

The unbalanced pressure source concept shows promise in the explanation of some features found in real data.

FURTHER WORK

The unbalanced pressure source idea must be investigated with methods that are closer to the reality of 3D data. Modelling in co-ordinates with the cylindrical axis down the borehole should be much better for the region near the source.

ACKNOWLEDGEMENTS

We would like to thank the sponsors of the CREWES project for their generous support.

REFERENCES

Hamarbitan, N.S. and Margrave, G.F., 2001, Spectral analysis of a ghost: Geophysics, **66**, 1267-1273.

Manning, P.M. and Margrave, G.F., 1998, Elastic wave finite-difference modelling as a practical exploration tool: CREWES 1998 Research Report; chapter 18.

FIGURES

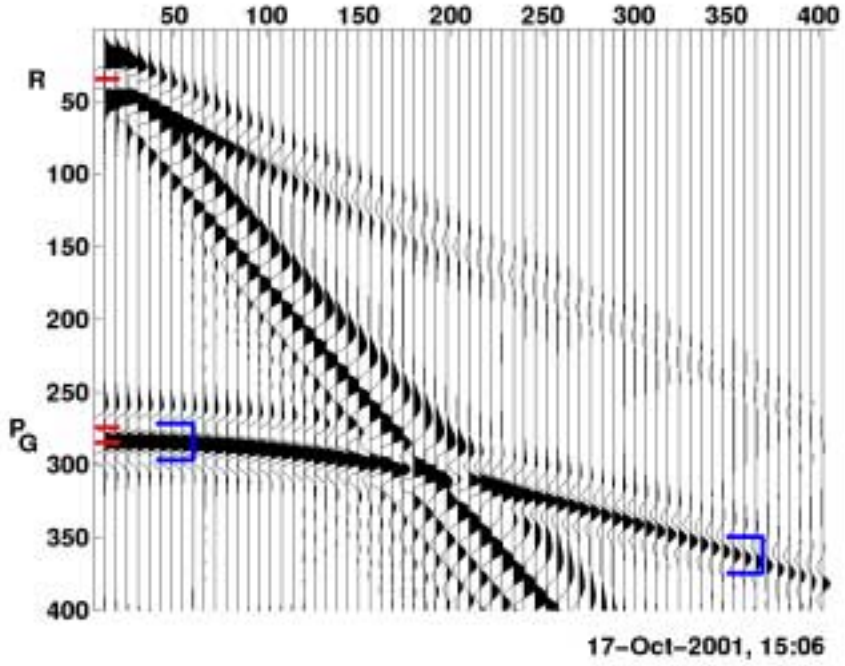

FIG. 1. A surface recording of the basic model with an 8-metre source. There is high amplitude ground roll but a high frequency reflection.

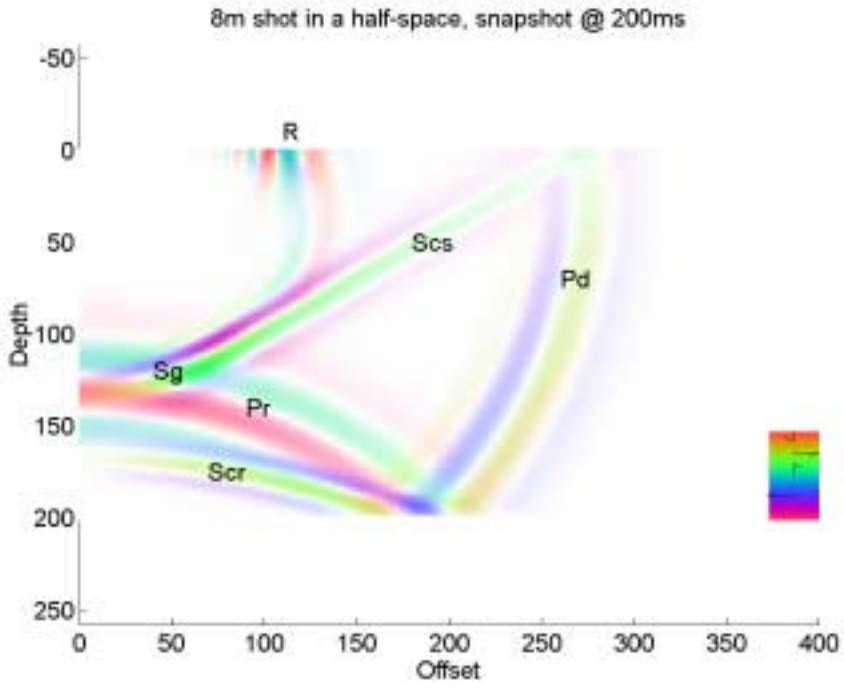

FIG. 2. A snapshot of the basic model with an 8-metre source. The three main types of wave are R (Rayleigh), P (Pressure), and S (Shear). See main text for details.

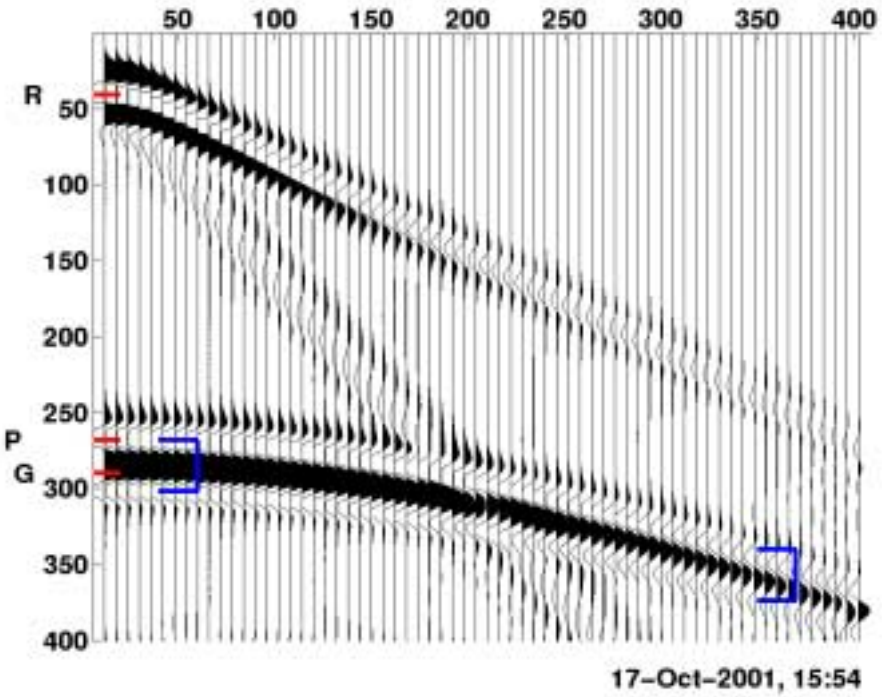

FIG. 3. A surface recording of the basic model with a source at 18 metres. The advantage of reduced ground roll is accompanied by the disadvantage of a lower frequency reflection. The reflection is actually a composite of the pressure-wave primary and ghost.

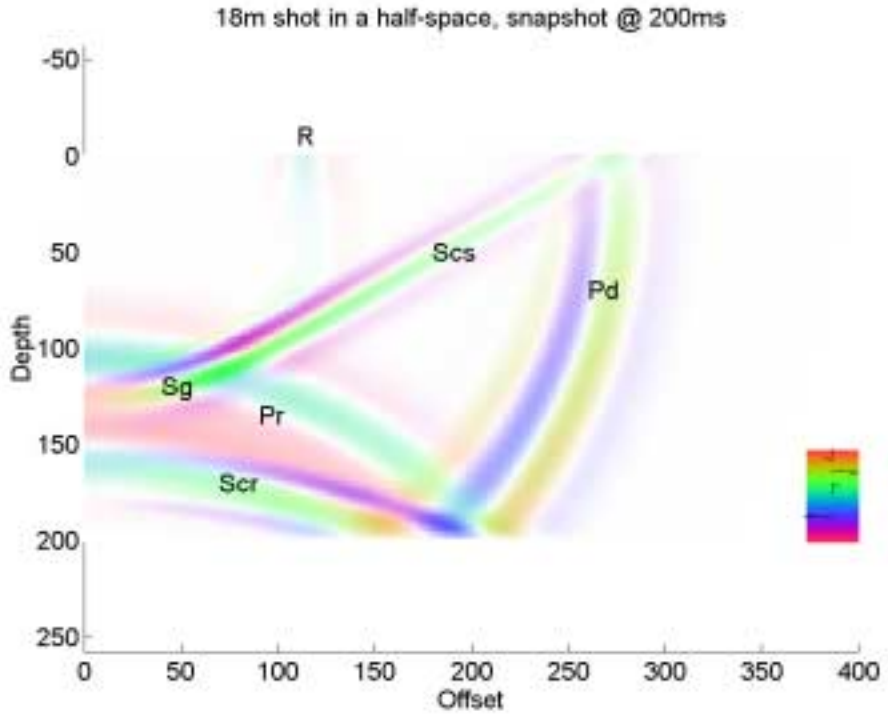

FIG. 4. A snapshot of the basic model with the source at 18 metres (case 2).

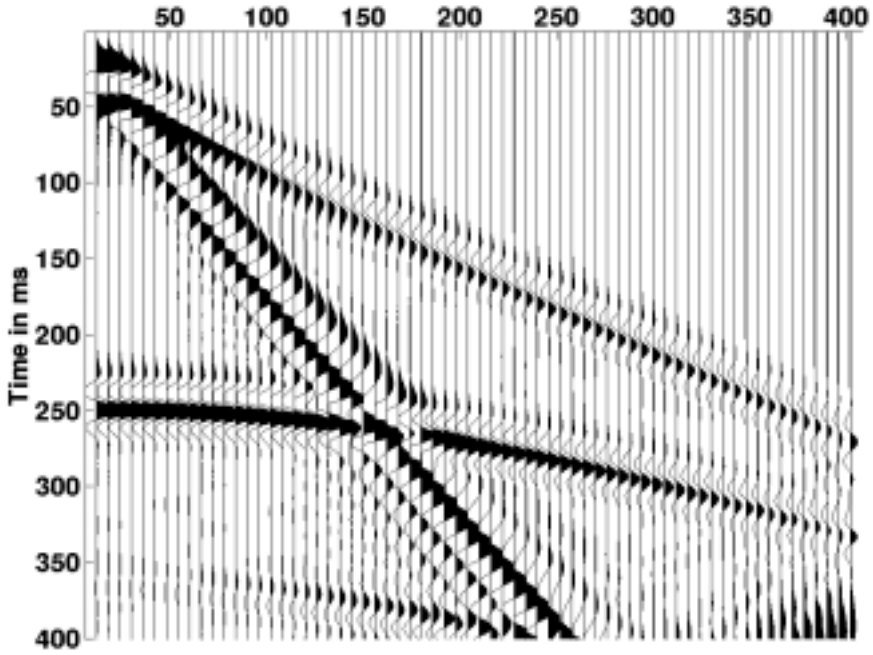

FIG. 5. A surface recording from the model of case 3. The first-break amplitudes are much higher because of the near-surface velocity gradient.

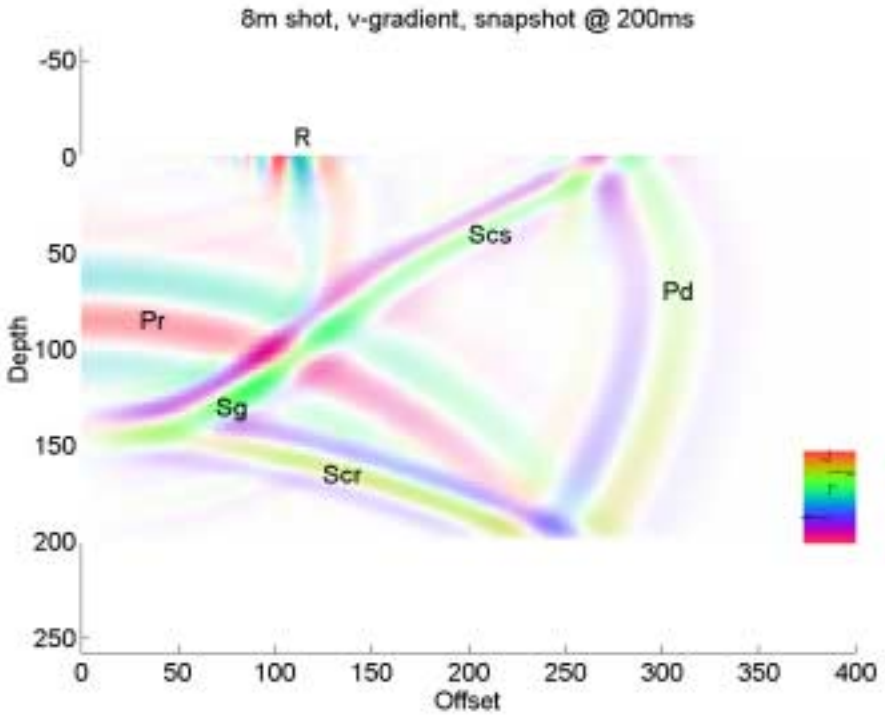

FIG. 6:.A snapshot of the case 3 model with a near-surface velocity gradient. The curved wave propagation caused by the velocity gradient provides much more energy to the first breaks.

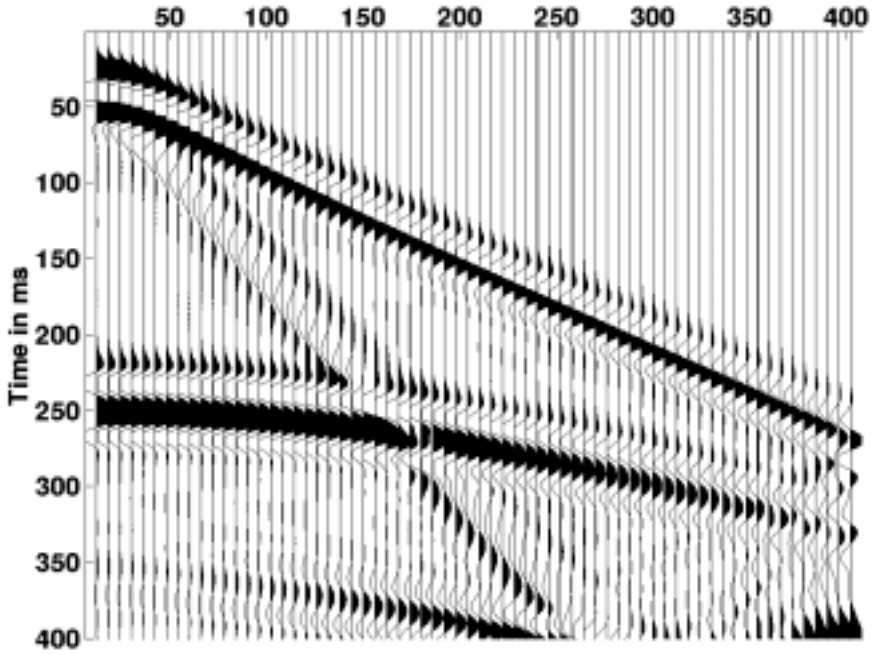

FIG 7. A surface recording from the deep-shot model of case 4. First-break amplitudes are again higher because of the near surface velocity gradient.

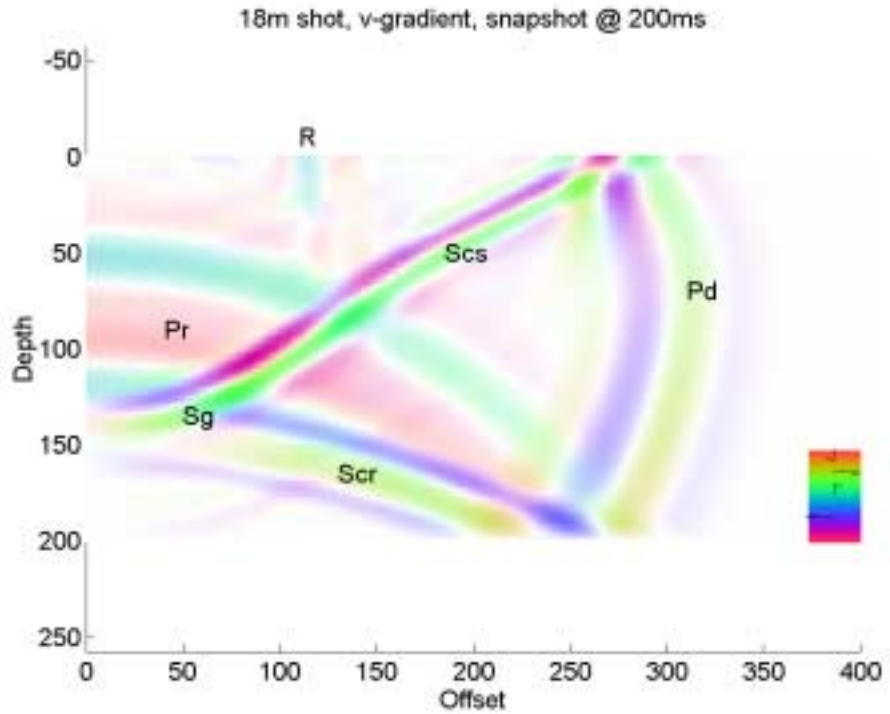

FIG 8. The case 4 snapshot at 200ms. Again, the upward propagation angle of the direct pressure wave near the surface provides high energy to the first breaks.

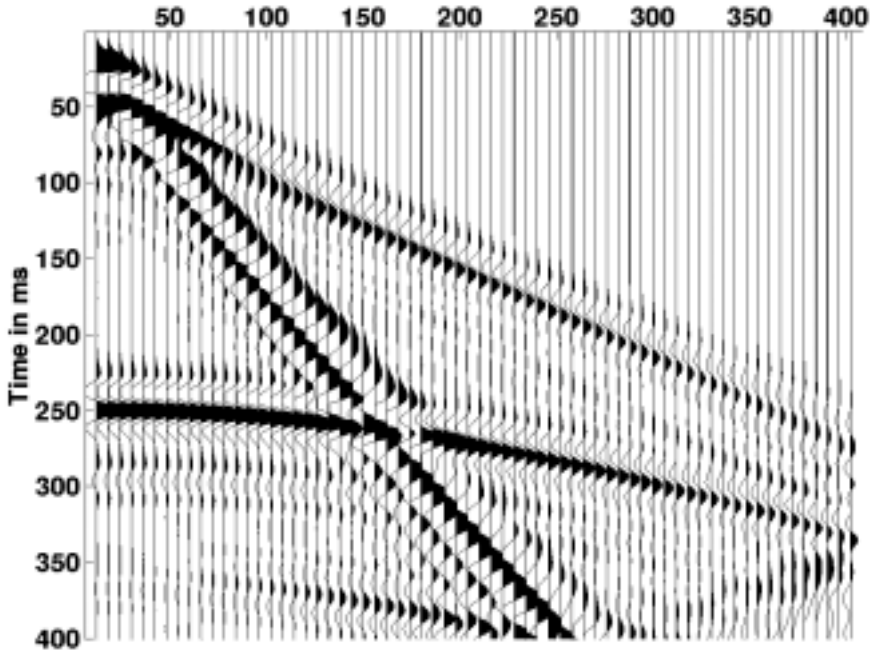

FIG. 9. The case 5 model of a shallow shot into the earth with a velocity step at 40m. Many features are similar to the velocity gradient case

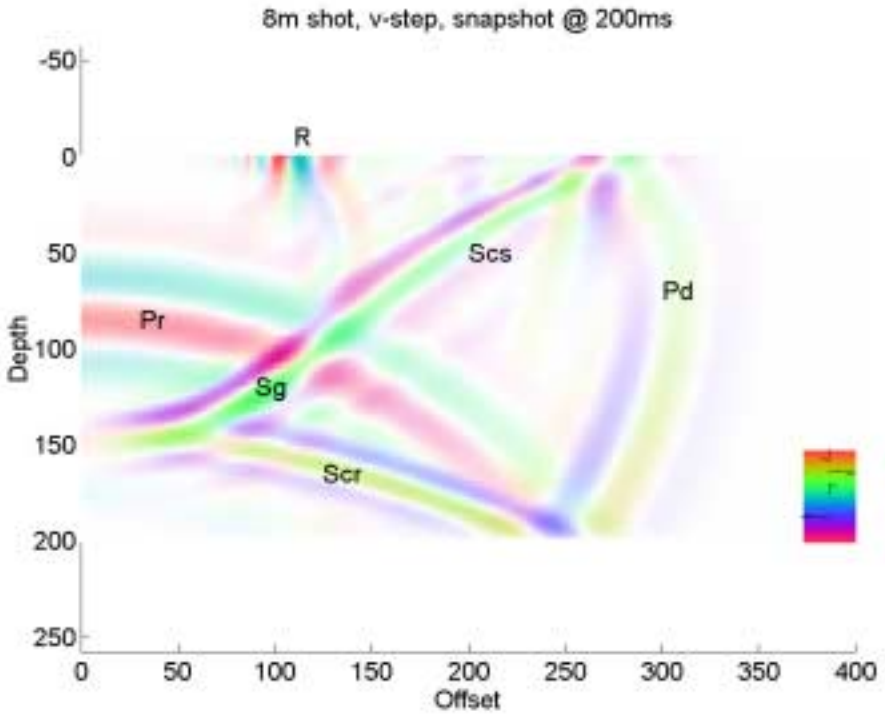

FIG. 10: The case 5 snapshot at 200ms. The similarity to the velocity gradient case can be seen, but multiple energy appears in various places.

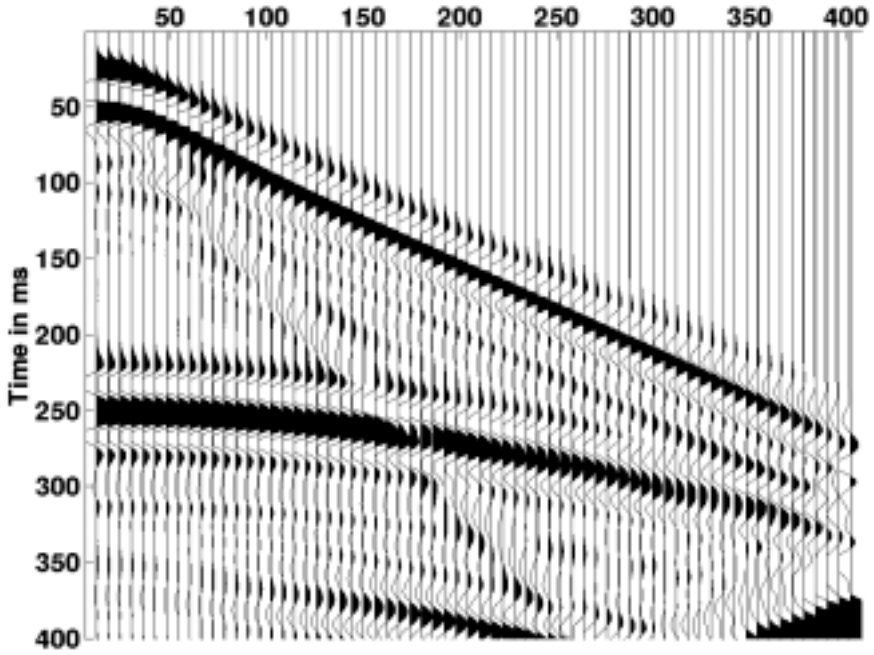

FIG. 11. The case 6 model of a deep shot into the earth with the velocity step at 40 m. The higher first-break amplitude makes the first-break multiple more obvious.

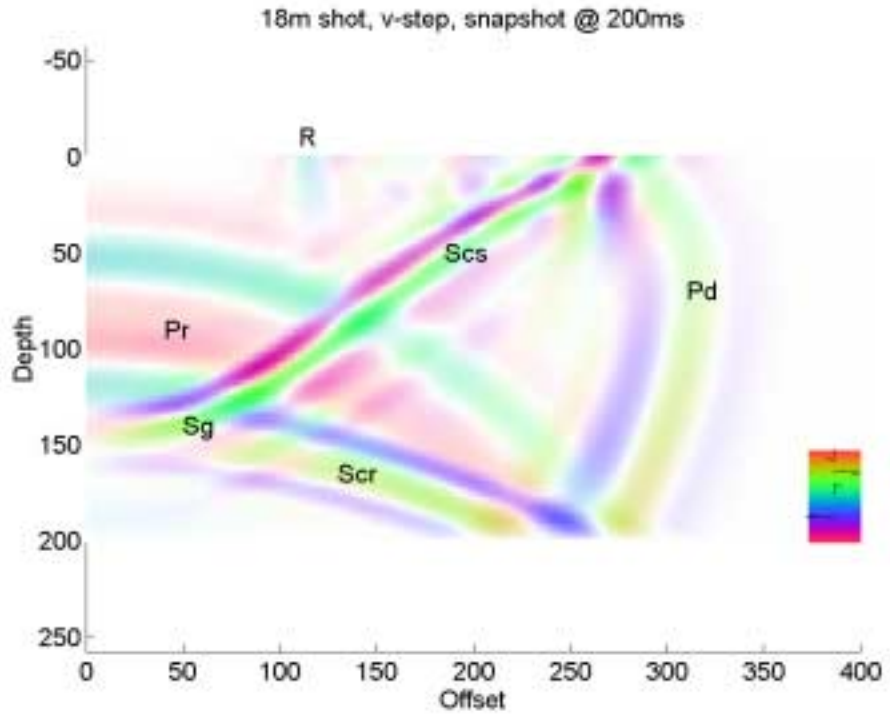

FIG. 12. The case 6 snapshot at 200ms. An additional ghost and P/S conversion from the shallow velocity step can be seen below the surface ghost and conversion.

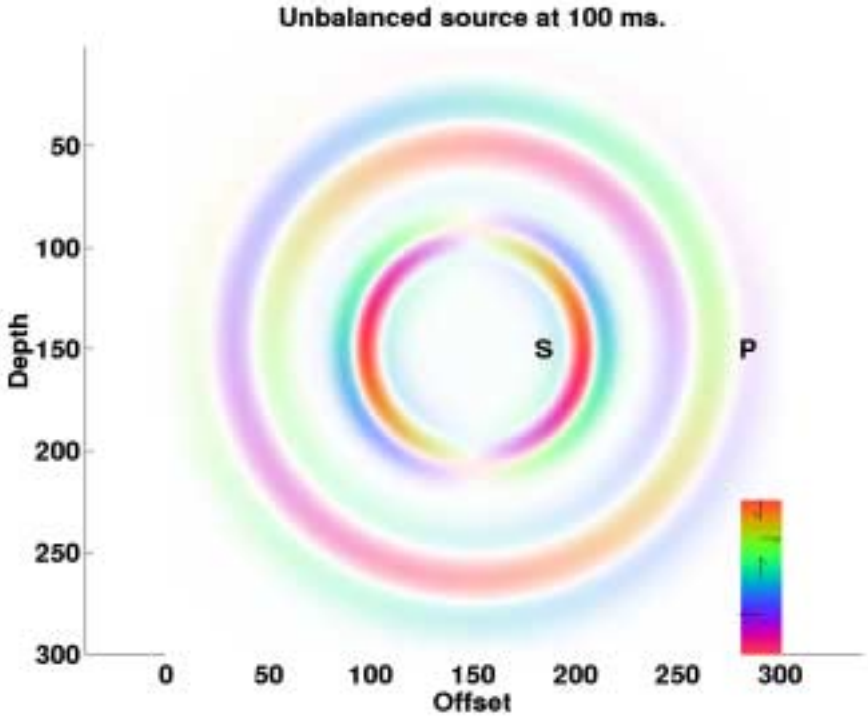

FIG. 13. An unbalanced source after propagation for 100ms. The outer wide rings are the pressure wave and the inner narrow rings are the split shear wave.

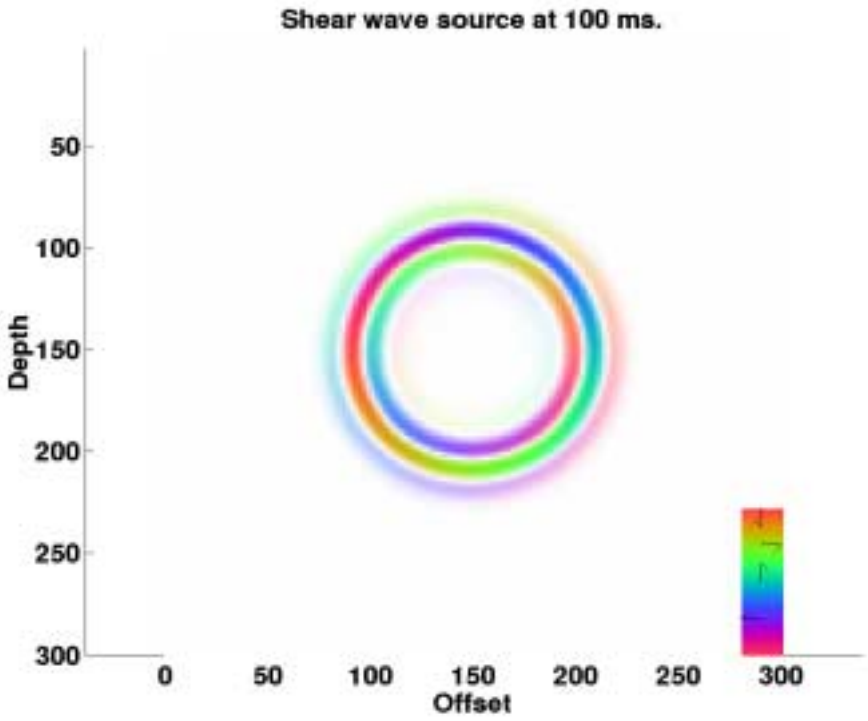

FIG. 14. A pure cylindrical shear-wave from the same frequency source as used to generate Figure 13. Comparison with this wave shows the split nature of the wave in Figure 13.

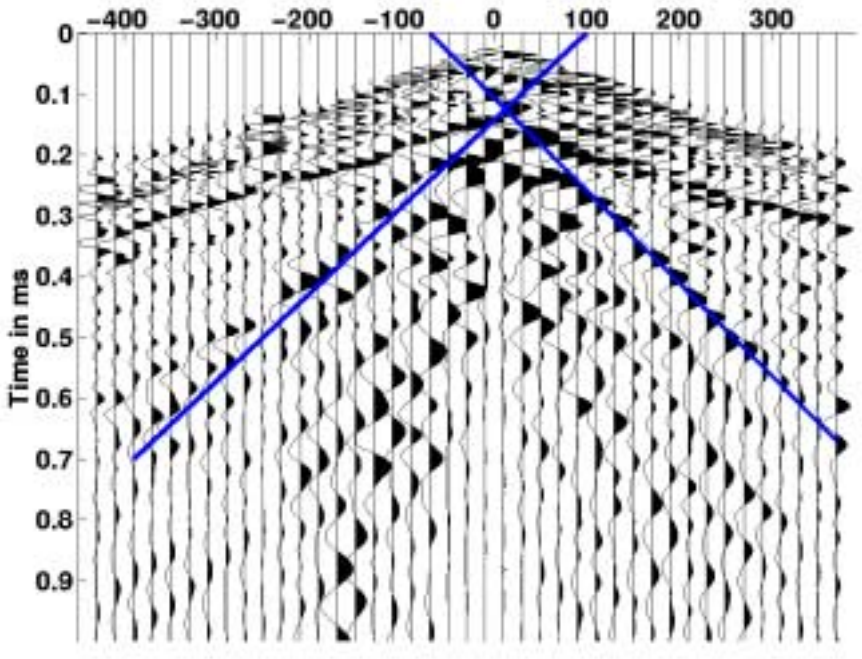

FIG. 15. A radial record from the Blackfoot area. The blue lines mark the candidates for unbalanced shear waves.

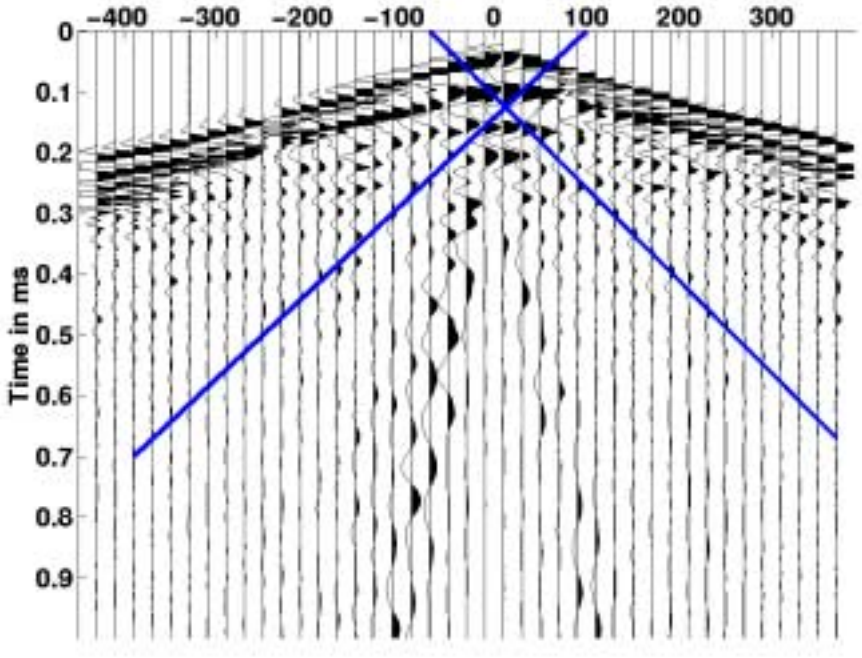

FIG. 16. The vertical record corresponding to Figure 11. Blue lines show the relatively low vertical energy of the events, and so they are not likely to be Rayleigh waves..

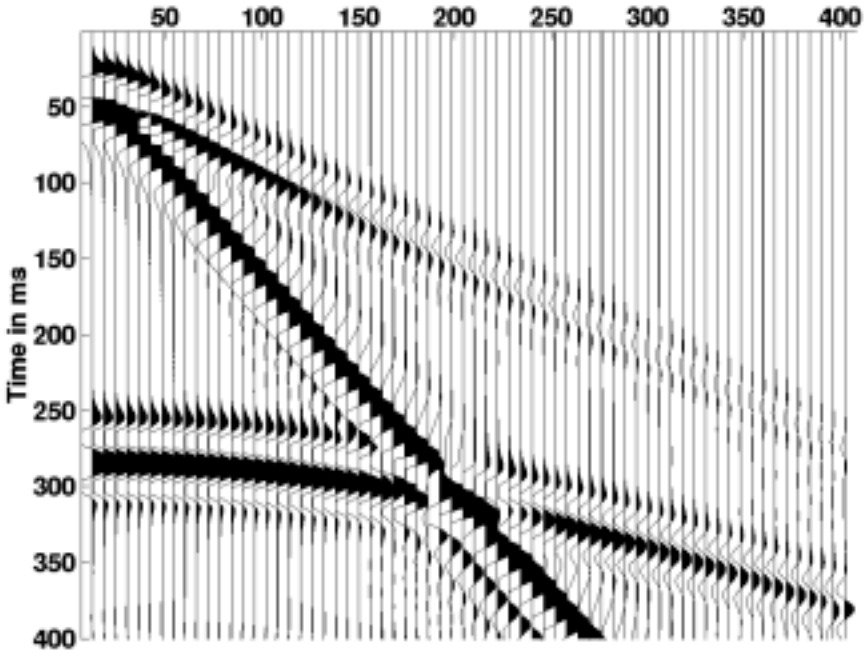

FIG. 17. An attempt to model the unbalanced source with parameters similar to the Blackfoot recording. The surface has converted almost all the shear energy into ground roll.